Korean J. Chem. Eng., **28**(12), 2236-2241 (2011)
DOI: 10.1007/s11814-011-0123-4

Influence of heat treatment on thermally-reduced graphene oxide/TiO_2 composites for photocatalytic applications

Thuy-Duong Nguyen-Phan, Viet Hung Pham, Hyunran Yun, Eui Jung Kim, Seung Hyun Hur, Jin Suk Chung, and Eun Woo Shin†

School of Chemical Engineering and Bioengineering, University of Ulsan, Daehakro 93, Nam-gu, Ulsan 680-749, Korea
(*Received 31 January 2011 • accepted 5 May 2011*)

Abstract–Thermally-reduced graphene oxide/TiO_2 composites (TRGO/Ti) were prepared by the thermal reduction of graphene oxide/TiO_2 composite that was obtained from a simple, environmentally friendly, one-step colloidal blending method. The changes in structural and textural properties as well as their corresponding photocatalytic activities were investigated as a function of calcination temperature. The presence of stacked TRGO sheets significantly retarded both the aggregation and the crystalline phase transformation of TiO_2 as increasing the temperature from 200 to 600 °C. TRGO/Ti composites exhibited higher photocatalytic activity for the degradation of methylene blue in comparison with pure TiO_2 due to the increase in specific surface area and the formation of π-π conjugations between dye compounds and aromatic regions of TRGO. However, increasing the calcination temperature resulted in the lower photoactivity and slower kinetics, which can be ascribed to the decrease in surface area, the reduction of oxygen vacancies, and the loss of functional groups at the edges or on the basal planes of the TRGO sheets.

Key words: TiO_2, Reduced Graphene Oxide, Nanocomposites, Dye, Photocatalytic Degradation, Porous Materials

INTRODUCTION

Wastewater produced in industrial processes including textile, pharmaceutical, paint, leather, and paper manufacturing contains several types of toxic and hazardous organic compounds, including dyestuffs and dyes that are suspected to be human carcinogens and strongly impact the environment [1]. Therefore, effective techniques for remediating dye compounds are necessary. Heterogeneous photocatalysis, an advanced oxidation process (AOP) using TiO_2-based materials as catalysts, is widely studied as a promising technology for water purification [2-5]. Work originating from the synthesis of hybrids or composites containing TiO_2 and carbon-based materials [6-9] that is related to the preparation of graphene-based composites with TiO_2 for photocatalytic applications was recently reported [10-14]. Graphene, a single atom-thick planar sheet of sp^2-bonded carbon atoms, has attracted scientific interest because of its outstanding electronic, mechanical, thermal and optical characteristics [15,16]. Graphene-based materials have been widely used as transparent conducting electrodes, supercapacitors, optoelectronic devices, composites, and catalysts [17-19]. Therefore, the preparation of reduced graphene oxide/TiO_2 composites may cause a synergistic effect that may potentially enhance the photodegradation of dye molecules due to the photoreactivity of TiO_2 itself [2-5] and the properties of reduced graphene oxide (RGO) [15-19].

Nevertheless, different variables that affected the structural and textural properties as well as the photocatalytic activity of such composites were well-investigated, including the precursor's type or concentration, graphene content, solvothermal temperature or time, reducing agent, preparation method, etc. [10-14,20-22]. However, to our best knowledge, the investigation of the effect of post-treatment temperature on the structure and photodegradation efficiency of the RGO/TiO_2 composite has not been accomplished yet.

In the present study, thermally-reduced graphene oxide/TiO_2 composites (TRGO/Ti) were prepared in two consequent simple steps. First, graphene oxide/TiO_2 composite containing 5 wt% of graphitic component was obtained by a colloidal blending method using commercial P25 and graphene oxide as the Ti precursor and carbonaceous sources. This is an environmentally friendly and easy method that preserves the interesting properties of TiO_2 as well as combines the fascinating properties of graphene oxide for stronger coupling effect. Subsequently, the as-synthesized composites underwent calcination to produce the thermally-reduced graphene oxide/TiO_2 composites. The composites' properties and photocatalytic activity were evaluated as a function of calcination temperature.

EXPERIMENTAL SECTION

The starting graphene oxide (GO) was prepared by a modified Hummers method using the expanded graphite [23]. Expanded graphite was produced by microwave-assisted heating the expandable graphite (grade 1721, Asbury Carbon). The exfoliated sheets were obtained during HCl-washing by deionized water and the final product was in the paste form with the concentration of 8.4 mg mL^{-1}. The detailed procedure was described in a previous report [24] and GO paste was then re-dispersed in 200 mL of deionized water. An aqueous dispersion of TiO_2 powder (Degussa, Germany) was added to the GO solution in which the nominal content of GO was 5 wt%. After sonication for 1.5 h and further stirring for 12 h at ambient conditions, the resulting grey product was filtered and dried in a

†To whom correspondence should be addressed.
E-mail: ewshin@mail.ulsan.ac.kr

vacuum at 50 °C for 4 h before being thermally treated for 2 h under Ar. The resulting samples were named TRGO/Ti-y, where "y" corresponds to the calcination temperature: 200, 400 and 600 °C.

The topography of starting GO material was observed by atomic force microscope (AFM) using a Veeco Dimension 3100 SPM (USA) with a silicon cantilever operated in the tapping mode. The structure, morphology and elemental distribution of the composites were recorded by FE-SEM (JEOL, JSM-600F, Japan) equipped with an energy-dispersive X-ray spectrometer (EDX) and high-resolution transmission electron microscope (HR-TEM, JEOL, JEM-2100F, Japan). Wide-angle XRD patterns were obtained on a Rigaku RAD-3C diffractometer (Japan) at 20 mA and 35 kV at a scan speed of 2°/min. Infrared spectra were measured by a Nicolet 380 FT-IR spectrometer (Thermo Electron Co., USA) using KBr pellet technique. The optical characteristics were obtained from UV-Vis-NIR spectrophotometer (HP 8453) using the normal incident transmittance. The BET surface area and pore volume of the materials were determined by N_2 adsorption/desorption measurement using a Micromeritics ASAP 2020 instrument (USA).

The photocatalytic activities were evaluated through the decomposition of 50 mL of an aqueous methylene blue solution (MB, C_o= 2.5×10^{-5} M, pH=5.85) in the presence of 10 mg of the composites. After dark adsorption, the solution containing photocatalyst was irradiated by four 20 W black lights (λ_{max}=352 nm) and four daylight (λ_{max}=545 nm) lamps (Alim Industry Co., Korea). The MB concentrations were determined by a UV-Vis absorbance microplate spectrophotometer (Spectra Max® Plus 384) with λ_{max}=664 nm as a function of irradiated time.

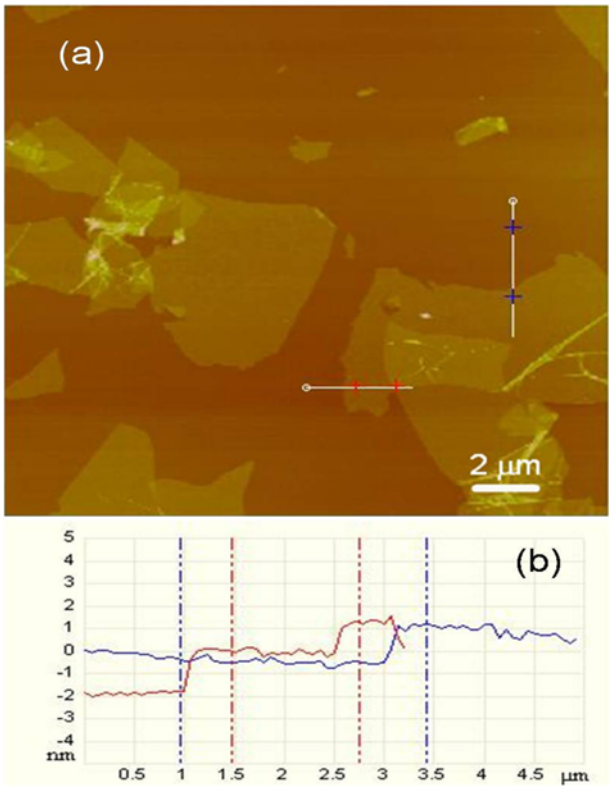

Fig. 1. (a) AFM topography image and (b) line profile of starting GO sheets deposited on silicon wafer from dispersion in water.

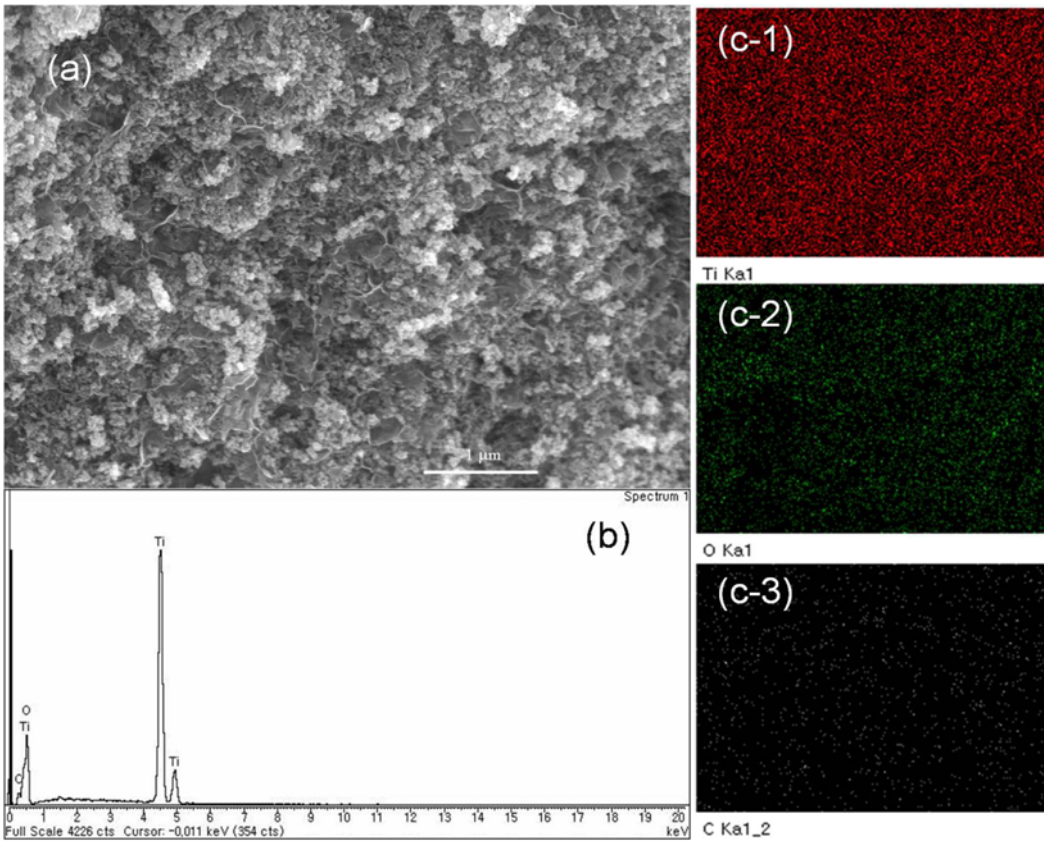

Fig. 2. (a) FE-SEM image, (b) EDX spectrum, and (c) mapping of the TRGO/Ti-600 sample.

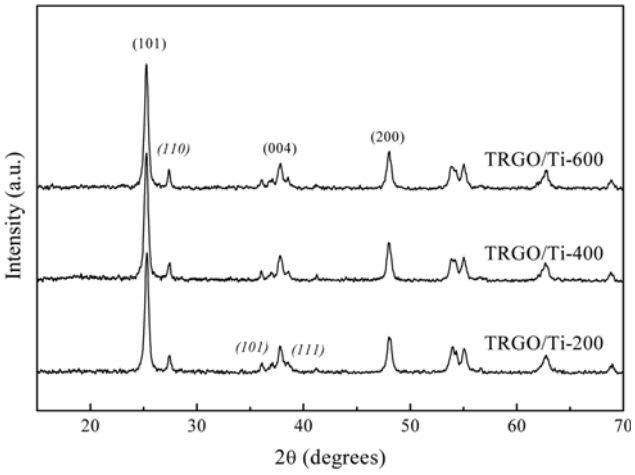

Fig. 3. XRD patterns of the TRGO/Ti-y samples.

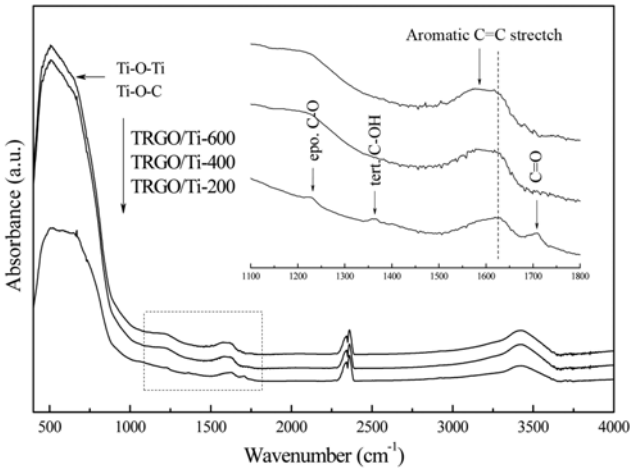

Fig. 5. FT-IR spectra of the TRGO/Ti-y samples.

RESULTS AND DISCUSSION

The starting GO dispersion in water was observed by AFM analysis as shown in Fig. 1. The topography image clearly illustrates the exfoliation of individual GO layer and the size of these large sheets is up to a few micrometers (Fig. 1(a)). The corresponding line profile reveals the thickness of a single-layer sheet ranging from 1.3 to 1.6 nm. The result is quite larger than that of individual pristine graphene sheet, ~0.34 nm, due to the presence of abundant oxygen-containing functional groups on the basal plane or at the edge of GO sheets [25]. The microstructure of the composites prepared from such GO sheets was characterized by electron microscope techniques. Fig. 2(a) shows representative FE-SEM images of the TRGO/Ti-600 composites, in which a crumpled stacking structure of TRGO/Ti-600 with wrinkles and folds, and abundant TiO_2 nanoparticles with sizes of 30-40 nm attached to it was observed. The elemental composition and distribution were analyzed by EDX spectra and mapping as displayed in Fig. 2(b) and 2(c). The Ti, O, and C components were distributed homogeneously and the C content was much less than the Ti and O contents in the composites.

The XRD results clearly indicated that the crystalline phase of TiO_2 was retained upon thermal treatment (Fig. 3). The lack of GO diffraction in the XRD patterns remarkably confirmed the exfoliation of TRGO sheets in the material. No remarkable differences in the intensities of the characteristic reflections, (101) and (200) for anatase with the $I4_1/amd$ structure (JCPDS 21-1272), as well as (110) and (101) for rutile indexing a symmetry group of $P4_2/mnm$ (JCPDS 21-1276) were observed. The anatase/rutile compositions, typically dominantly ~80% of anatase, also remained despite various thermal treatment temperatures. Herein, it clearly demonstrates that the presence of TRGO significantly inhibited TiO_2 aggregation and suppressed the phase transformation at high temperature that usually occurs with calcined TiO_2 nanoparticles [26-28]. These results are well consistent with the observation from HR-TEM analysis displayed in Fig. 4, in which the unchanged particle size of TiO_2 in the composites was obtained as increasing the temperature from 200 to 600 °C. Additionally, TiO_2 particles in irregular geometry, including quasi-cubic and granular shapes, were realized in Fig. 4(b) and the lattice spacing of 0.35 nm was assigned to the (101) plane of highly crystalline anatase phase, being in good agreement with the XRD results aforementioned.

The changes in the functional groups upon heat treatment were confirmed in the FT-IR spectra (Fig. 5), in which broad peaks at ~3,400 cm^{-1} and in the range of 400-1,000 cm^{-1} were observed in

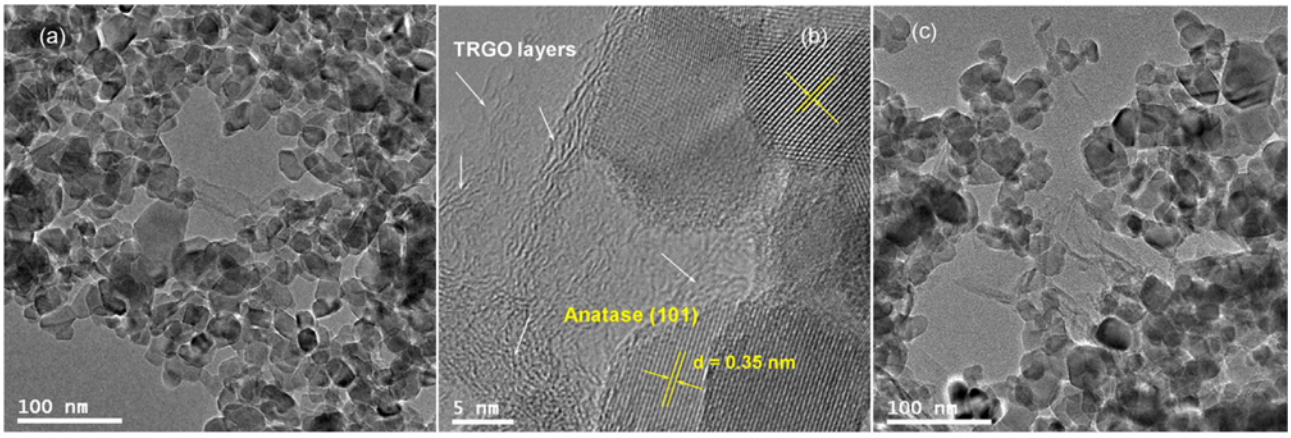

Fig. 4. HR-TEM images of (a), (b) TRGO/Ti-200 and (c) TRGO/Ti-600 composites.

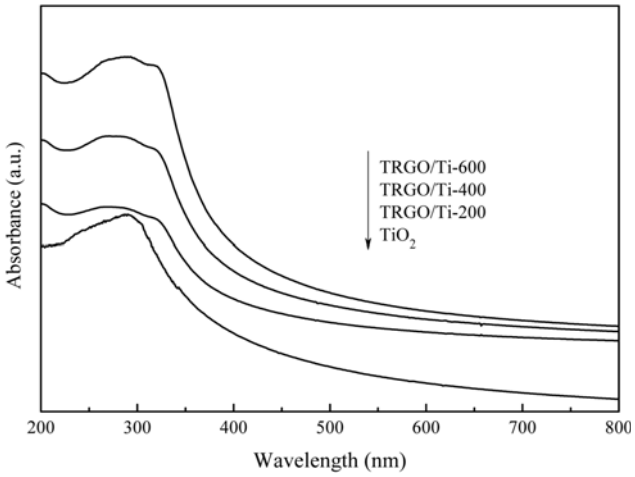

Fig. 6. UV-Vis absorption spectra of TiO_2 and TRGO/Ti-y.

all samples, implying the existence of surface O-H stretching vibration and Ti-O-Ti/Ti-O-C bonding, respectively. The absorption band at 1,710 cm^{-1}, characteristic of C=O stretching of the carboxylic groups at the edges of the TRGO sheets, was observed in the TRGO/Ti-200 sample but not in the other samples. Similarly, small traces of tertiary C-OH and epoxy C-O at 1,385 and 1,230 cm^{-1}, respectively, existed only in the TRGO/Ti-200 sample. All oxygen-containing functional groups disappeared after thermal reduction at 400 and 600 °C. Additionally, the new broad peaks in the range of 1,550-1,670 cm^{-1}, which slightly shifted to the shorter region at higher temperature, can be assigned to the indicative skeletal vibration of reduced graphene, denoted as conjugated C=C [11].

Fig. 6 illustrated the UV-Vis-NIR absorption spectra of TiO_2 and TRGO/Ti-y composites. It can be seen that the absorption edges of the composites remarkably red-shifted from 400 nm to 440 nm in comparison with pure TiO_2, demonstrating the narrowing of the band gap energy of TiO_2 by TRGO incorporation that generates Ti-O-C chemical bonding in the composites. However, gradually increasing the heat treatment temperature resulted in the blue-shift from 440 nm to 430 and 415 nm, proposing the weaker utilization of visible light for TRGO/Ti-400 and TRGO/Ti-600.

Beside the changes in optical properties, the influence of calcination temperature on the textural characteristics of the composites was also proven. The specific surface areas and pore volumes of

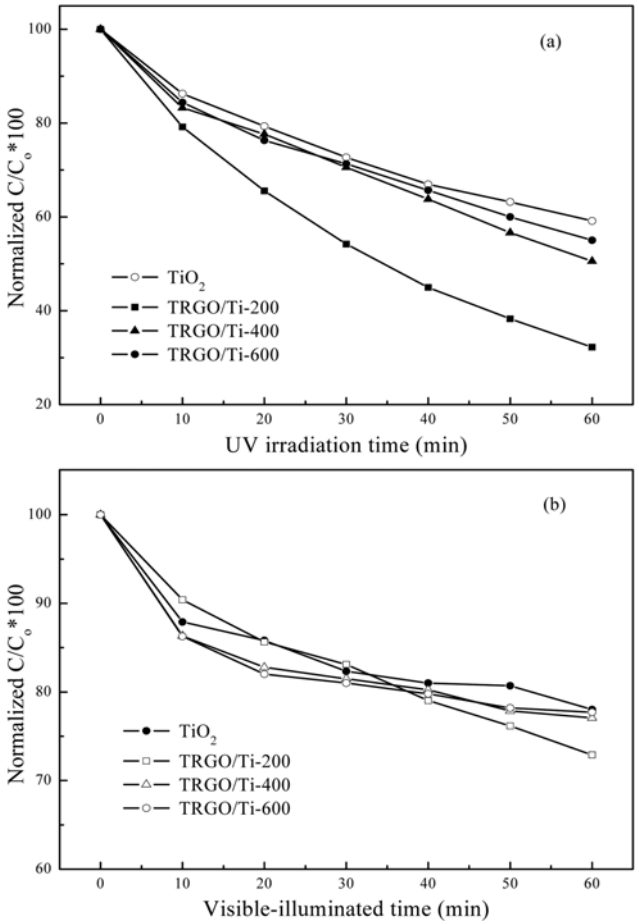

Fig. 7. Photodecomposition results of MB using pure TiO_2 and TRGO/Ti-y composites under (a) UV and (b) visible illuminations.

the composites were determined by N_2 sorption measurements. As seen in Table 1, the porosity of TRGO/Ti-y gradually decreased with increasing calcination temperature, but was much higher than that of pure TiO_2. The TRGO/Ti-200 composites exhibited the largest specific surface area and pore volume of 72.9 m^2 g^{-1} and 0.4739 cm^3 g^{-1}, respectively, which can be attributed to the strict and tight stacking of TRGO nanosheets due to the van der Waal forces at high temperature, the increase in hydrophobicity, and the gradual

Table 1. Porosity characteristics and kinetic parameters of MB photodegradation with irradiated TRGO/Ti-y composites

Sample	S_{BET} (m^2 g^{-1})[a]	V_t (cm^3 g^{-1})[a]	X (%)[b]		k_{app} (min^{-1}) ($\times 10^{-3}$)[c]		R[d]	
			UV	Vis	UV	Vis	UV	Vis
TiO_2	43.99	0.1501	40.86	21.99	8.48	3.48	-	-
TRGO/Ti-200	72.92	0.4739	67.76	27.11	18.66	4.90	2.22	1.41
TRGO/Ti-400	64.92	0.4359	49.43	22.91	10.76	3.63	1.27	1.04
TRGO/Ti-600	59.44	0.3984	44.97	22.29	9.37	3.50	1.13	1.01

[a]Specific surface area and pore volume as determined by N_2 sorption analysis

[b]Final conversion X(%)=[1−(C/C_o)]*100 where C_o and C are the initial MB concentration and the concentration at the irradiation time t, respectively

[c]Apparent first-order rate constant (min^{-1}) evaluated from the slope of the plot of ln(C/C_o)=− k_{app}t

[d]Synergy factor, R=k_{app}(TRGO/Ti-y)/k_{app}(TiO_2)

loss of oxygen-containing functional groups at the edges or on the surfaces of graphitic layers. Otherwise, as mentioned above, numerous studies demonstrated that the heat treatment significantly reduced TiO_2 surface area and broadened the particle size due to the aggregation phenomenon [26-28]. However, in the present study, which relied on HR-TEM and XRD results, the porosity suppression was negligibly affected by TiO_2 themselves and the most important factor that influenced the porosity of the composites is the thermal reduction of GO to TRGO.

Subsequently, the effects of heat treatment on the photocatalytic activities of the TRGO/Ti-y composites were evaluated with the decomposition of an aqueous MB solution. Fig. 7(a) shows the photocatalytic degradation of MB under UV irradiation after dark adsorption. The MB photocatalytic activities over the composite catalysts were higher than MB photocatalytic activities over pure TiO_2 and decreased with increasing calcination temperature. This finding may be explained by the effective role of TRGO in MB decolorization. Typically, about 70% of the MB was decomposed with the TRGO/Ti-200 sample within 1 h of UV-exposure, whereas about 50-60% of the MB remained when using pure TiO_2 and the other composites as the photocatalysts. The removal activity gradually decreased with increasing the calcination temperature. However, no different efficiency was observed irrespective of pure TiO_2 or composite materials in the case of using visible source, although ~30% of MB was decolorized after 1 h (Fig. 7(b)), indicating that the composites did not work well at longer wavelength region.

As seen in Fig. 8(a), the linear transformation of $\ln(C/C_o)=-k_{app}t$ clearly demonstrates that the net UV-photodegradation behavior of TiO_2 and TRGO/Ti-y composites follows the Langmuir-Hinshelwood pseudo-first-order kinetic model [29-32]. The apparent reaction rate constant (k_{app}) values achieved from the slope of the linear regression analysis are given in Table 1. The photocatalytic degradation rate decreased in the order of TRGO/Ti-200>TRGO/Ti-400>TRGO/Ti-600>TiO_2, in which the fastest rate was about 18.66×10^{-3} min^{-1} that are comparable to the previous studies [11-14,20-22]. However, low correlation coefficients were attained from the linear plots of the materials which worked under visible illumination although the same trend was found for the decomposition order (Fig. 8(b)). It implies that both pure TiO_2 and the prepared composites do not obey the first-order kinetic model as the case of visible light-irradiation. The results are quite consistent with the optical properties observed before. Moreover, a synergy factor (R) defined as $R= k_{app}(xGO/Ti)/k_{app}(TiO_2)$ was also estimated to quantify the extent of the synergy effect of TRGO/Ti-y composites compared to pure TiO_2 [29]. The apparent rate constant has been chosen as the basic kinetic parameter to compare the different systems because it is independent of the concentration and, thus, enables one to determine the photocatalytic activity independently of the previous adsorption period in the dark [29]. Correspondingly, as described in Table 1, the estimated R value decreased from 2.22 and 1.55 for TRGO/Ti-200 to 1.13 and 1.09 for TRGO/Ti-600 irradiated under UV light, indicating a decrease in the synergistic effect of TRGO upon heat treatment.

The experimental results demonstrate the additive function of TRGO in photocatalytic applications, in which the presence of TRGO sheets enhances the specific surface area to facilitate the efficient diffusion, adsorption, and subsequent decomposition of MB. The decrease in MB photodegradation with the TRGO/Ti-y composites with increasing calcination temperature can be attributed to a reduction in porosity and, therefore, to a decrease in adsorbability. Moreover, as illustrated in Fig. 9, the loss of oxygen-containing functional groups as GO was transformed into thermally-reduced GO,

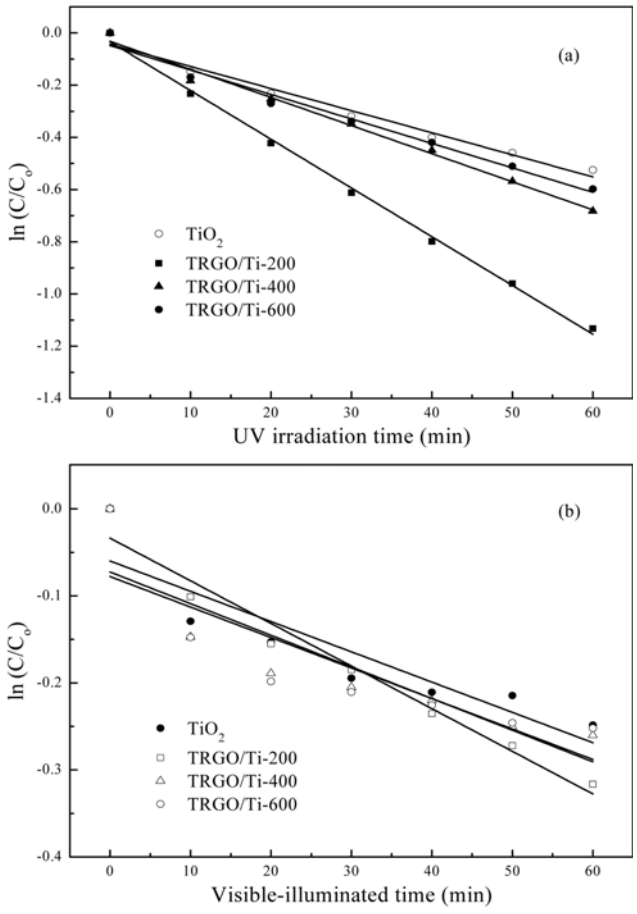

Fig. 8. Plots of the apparent first-order linear transform $\ln(C/C_o)$ vs. the illumination time upon (a) UV and (b) visible lights.

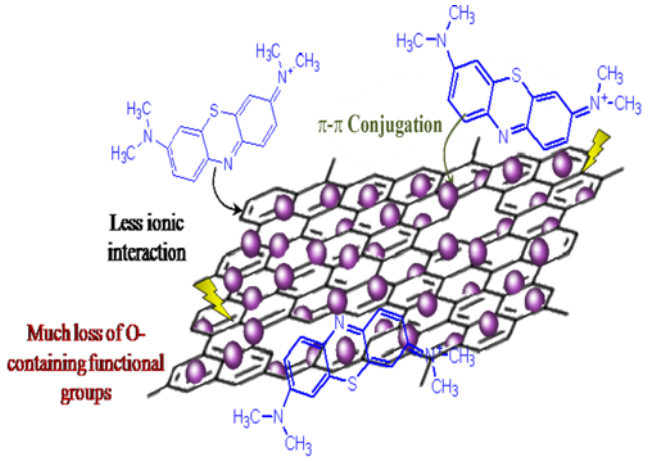

Fig. 9. Proposed interactions between TiO_2/thermally-reduced GO and MB (violet - TiO_2 particles, black - TRGO sheet, blue - MB molecules).

likely enhancing the hydrophobicity as well as weakening the ionic interactions and formation of π-π conjugations between the dye and TRGO nanosheets. Those phenomena negatively impacted the photodecomposition over the composites calcined at higher temperature. The photodegradation can also be attributed to the generation of oxygen vacancies formed in a vacuum environment due to the interactions between free carbon and oxygen in TiO_2 [12,33]. Because the GO : TiO_2 mass ratio was unchanged, increasing the calcination temperature resulted in a lower carbon content due to a higher reduction efficiency of GO to TRGO, thus reducing the oxygen vacancies in the TRGO/Ti-y composites. These oxygen defects act as electron traps, retarding the recombination of electron-hole pairs and thus enhancing photodegradation. Fewer vacancies were generated with higher calcination temperatures, leading to decreases in removal efficiency.

CONCLUSIONS

Thermally-reduced graphene oxide/titania composites were synthesized using a simple, environmentally friendly, one-step colloidal blending method. The presence of stacked TRGO sheets significantly suppressed the aggregation and crystalline phase transformation of TiO_2 as the calcination temperature increased. The TRGO/Ti-y composites exhibited higher photocatalytic degradation of MB compared to pure TiO_2. Lower decomposition efficiencies and slower kinetics were obtained at higher calcination temperatures.

ACKNOWLEDGEMENTS

This research was supported by the Basic Science Research Program through the National Research Foundation of Korea (NRF) funded by the Ministry of Education, Science and Technology (2010-0008810).

REFERENCES

1. M. A. Brown and S. C. De Vito, *Crit. Rev. Environ. Sci. Technol.*, **23**, 249 (1993).
2. A. L. Linsebigler, G. Lu and J. T. Yates Jr., *Chem. Rev.*, **95**, 735 (1995).
3. M. R. Hoffmann, S. T. Martin, W. Y. Choi and D. W. Bahnemann, *Chem. Rev.*, **95**, 69 (1995).
4. X. Chen and S. S. Mao, *Chem. Rev.*, **107**, 2891 (2007).
5. R. Thiruvenkatachari, S. Vigneswaran and I. S. Moon, *Korean J. Chem. Eng.*, **25**, 64 (2008).
6. X.-H. Xia, Z.-J. Jia, Y. Yu, Y. Liang, Z. Wang and L.-L. Ma, *Carbon*, **45**, 717 (2007).
7. Y. Li, S. Sun, M. Ma, Y. Ouyang and W. Yan, *Chem. Eng. J.*, **142**, 147 (2008).
8. J. Shi, J. Zheng, P. Wu and X. Ji, *Catal. Commun.*, **9**, 1846 (2008).
9. S.-M. Lam, J.-C. Sin and A. R. Mohamed, *Korean J. Chem. Eng.*, **27**, 1109 (2010).
10. O. Akhavan and E. Ghaderi, *J. Phys. Chem. C*, **113**, 20214 (2009).
11. H. Zhang, X. Lv, Y. Li, Y. Wang and J. Li, *ACS Nano*, **4**, 380 (2010).
12. X.-Y. Zhang, H.-P. Li, X.-L. Cui and Y. Lin, *J. Mater. Chem.*, **20**, 2801 (2010).
13. Y. Wang, R. Shi, J. Lin and Y. Zhu, *Appl. Catal. B Environ.*, **100**, 179 (2010).
14. K. Zhou, Y. Zhu, X. Yang, X. Jiang and C. Li, *New J. Chem.*, **35**, 353 (2011).
15. M. I. Katsnelson, *Mater. Today*, **10**, 20 (2007).
16. A. K. Geim and K. S. Novoselov, *Nat. Mater.*, **6**, 183 (2007).
17. M. D. Stoller, S. Park, Y. Zhu, J. An and R. S. Ruoff, *Nano Lett.*, **8**, 3498 (2008).
18. P. Blake, P. D. Brimicombe, R. R. Nair, T. J. Booth, D. Jiang, F. Schedin, L. A. Ponomarenko, S. V. Morozov, H. F. Gleeson, E. W. Hill, A. K. Geim and K. S. Novoselov, *Nano Lett.*, **8**, 1704 (2008).
19. K. S. Kim, Y. Zhao, H. Jang, S. Y. Lee, J. M. Kim, K. S. Kim, J.-H. Ahn, P. Kim, J.-Y. Choi and B. H. Hong, *Nature*, **457**, 706 (2009).
20. T. N. Lambert, C. A. Chavez, B. Hernandez-Sanchez, P. Lu, N. S. Bell, A. Ambrosini, T. Friedman, T. J. Boyle, D. R. Wheeler and D. L. Huber, *J. Phys. Chem. C*, **113**, 19812 (2009).
21. D. Wang, D. Choi, J. Li, Z. Yang, Z. Nie, R. Kou, D. Hu, C. Wang, L. V. Saraf, J. Zhang, I. A. Aksay and J. Liu, *ACS Nano*, **3**, 907 (2009).
22. P. Wang, Y. Zhai, D. Wang and S. Dong, *Nanoscale*, **3**, 1640 (2011).
23. W. S. Hummers Jr. and R. E. Offeman, *J. Am. Chem. Soc.*, **80**, 1339 (1958).
24. V. H. Pham, T. V. Cuong, S. H. Hur, E. W. Shin, J. S. Kim, J. S. Chung and E. J. Kim, *Carbon*, **48**, 1945 (2010).
25. S. Stankovich, D. A. Dikin, R. D. Piner, K. A. Kohlhaas, A. Kleinhammes, Y. Jia, Y. Wu, S. T. Nguyen and R. S. Ruoff, *Carbon*, **45**, 1558 (2007).
26. J. Yu, J. C. Yu, W. Ho and Z. Jiang, *New J. Chem.*, **26**, 607 (2002).
27. C. Rath, P. Mohanty, A. C. Pandey and N. C. Mishra, *J. Phys. D: Appl. Phys.*, **42**, 205101 (2009).
28. A. Nakaruk, C. Y. Lin, D. S. Perera and C. C. Sorrell, *J. Sol-Gel Sci. Technol.*, **55**, 328 (2010).
29. J. Matos, J. Laine and J.-M. Herrmann, *Appl. Catal. B Environ.*, **18**, 281 (1998).
30. A. Houas, H. Lachheb, M. Ksibi, E. Elaloui, C. Guillard and J.-M. Herrmann, *Appl. Catal. B: Environ.*, **31**, 145 (2001).
31. T.-W. Kim, M.-J. Lee, W.-G. Shim, J.-W. Lee, T.-Y. Kim, D.-H. Lee and H. Moon, *J. Mater. Sci.*, **43**, 6486 (2008).
32. Y. Yao, G. Li, S. Ciston, R. M. Lueptow and K. A. Gray, *Environ. Sci. Technol.*, **42**, 4952 (2008).
33. P. W. Chou, Y. S. Wang, C. C. Lin, Y. J. Chen, C. L. Cheng and M. S. Wong, *Surf. Coat. Technol.*, **204**, 834 (2009).